Acta Biomaterialia 10 (2014) 680–687

Contents lists available at ScienceDirect

Acta Biomaterialia

journal homepage: www.elsevier.com/locate/actabiomat

A polymeric device for controlled transscleral multi-drug delivery to the posterior segment of the eye

Nobuhiro Nagai [a], Hirokazu Kaji [b], Hideyuki Onami [a,c], Yumi Ishikawa [a], Matsuhiko Nishizawa [b], Noriko Osumi [d], Toru Nakazawa [c], Toshiaki Abe [a,*]

[a] Division of Clinical Cell Therapy, United Centers for Advanced Research and Translational Medicine (ART), Tohoku University Graduate School of Medicine, 2-1 Seiryo-machi, Aoba-ku, Sendai 980-8575, Japan
[b] Department of Bioengineering and Robotics, Graduate School of Engineering, Tohoku University, 6-6-01 Aramaki, Aoba-ku, Sendai 980-8579, Japan
[c] Department of Ophthalmology, Tohoku University Graduate School of Medicine, 1-1 Seiryo-machi, Aoba-ku, Sendai 980-8574, Japan
[d] Division of Developmental Neuroscience, United Centers for Advanced Research and Translational Medicine (ART), Tohoku University Graduate School of Medicine, 2-1 Seiryo-machi, Aoba-ku, Sendai 980-8575, Japan

ARTICLE INFO

Article history:
Received 28 August 2013
Received in revised form 26 October 2013
Accepted 8 November 2013
Available online 15 November 2013

Keywords:
Transscleral delivery
Multi-drug delivery
Retina
Poly(ethyleneglycol) dimethacrylate

ABSTRACT

The design of drug delivery systems that can deliver multiple drugs to the posterior segment of the eye is a challenging task in retinal disease treatments. We report a polymeric device for multi-drug transscleral delivery at independently controlled release rates. The device comprises a microfabricated reservoir, controlled-release cover and three different fluorescent formulations, which were made of photopolymeized tri(ethyleneglycol)dimethacrylate (TEGDM) and poly(ethyleneglycol)dimethacrylate (PEGDM). The release rate of each fluorescent is controlled by varying the PEGDM/TEGDM ratio in its formulation and the cover. The release kinetics appeared to be related to the swelling ratio of the PEGDM/TEGDM polymers. When the devices were implanted onto rat sclerae, fluorescence was observable in the ocular tissues during 4 weeks' implantation and distributed locally around the implantation site. Our polymeric system, which can administer multiple compounds with distinct kinetics, provides prolonged action and less invasive transscleral administration, and is expected to provide new tools for the treatment of posterior eye diseases with new therapeutic modalities.

1. Introduction

Diseases of the posterior eye segments cause impaired vision and blindness for millions of patients around the world [1]. There has been an increase in the understanding of the disease processes, and multiple factors have been reported to play a role in the diseases [2–4]. Thus, multi-drug therapy has become the primary method of disease management, because it offers the major advantages of enhanced efficacy of treatment, reduction of each drug dose, and mitigation of toxicity and side-effects caused by high doses of single drugs [5–7]. Multiple drugs have been used to treat patients with glaucoma [5,6] and to suppress choroidal neovascularization in patients with age-related macular degeneration (AMD) [7]. The regulation of neovascularization has received much attention, and it is now known that its balance is maintained by more than two dozen cytokines [8]. Thus it would be more effective and reasonable to use a number of drugs to treat such disease processes. Some techniques and novel pharmacological agents offer promise for the future treatment of posterior eye segment diseases [9–11]. However, the successful treatment of some retinal diseases has been limited. The limitation may be partially related to inadequate drug delivery systems for the retina, including multiple drug administration.

The principal route for local ophthalmic drug delivery remains topical application [12]. However, drug delivery to intraocular tissue by this approach is limited by the significant barrier of corneal epithelium and tear fluid turnover [13]. Systemic drug administration is not a viable alternative due to the blood–retinal barrier that limits drug access to the posterior tissues of the eye. Although intravitreal injections and intraocular implants may deliver drugs effectively to the retina and choroid, this approach is invasive to the eye and may cause severe adverse effects, such as endophthalmitis and retinal detachment [14]. Periocular or transscleral routes are less invasive than intravitreal administration and provide higher retinal and vitreal drug bioavailability (~0.01–0.1%) compared to eye drops (about 0.001% or less) [15,16]. Due to the high degree of hydration and low cell density of the sclera, soluble substrates readily pass through the sclera, although the ease of penetration of the drug to the vitreous cavity is dependent on the thickness

* Corresponding author. Tel./fax: +81 22 717 8234.
E-mail address: toshi@oph.med.tohoku.ac.jp (T. Abe).

1742-7061/$ - see front matter © 2013 Acta Materialia Inc. Published by Elsevier Ltd. All rights reserved.
http://dx.doi.org/10.1016/j.actbio.2013.11.004

of the sclera [17]. Thus transscleral delivery has the potential to be a more effective and less invasive route for intraocular drug delivery.

Several potential carriers for ocular drug delivery such as micelles [18], microneedles [19], nano- or microparticles [20,21], liposomes [22,23] and hydrogel systems [24,25] have been investigated. All the systems are injectable for localized and targeted delivery of drugs to the desired site and biodegradable to avoid a second procedure for implant removal. However, release profiles for biodegradable systems are generally complex with burst effects, i.e. an initial burst, a diffusional release phase and a final burst [26]. Additionally, the release period of such biodegradable systems is limited to less than 2 weeks [25]. In chronic eye diseases such as AMD and retinitis pigmentosa, duration of effect with controlled drug release is critical. Although several systems for multi-drug delivery have been developed [27–32], there are none intended for ocular multi-drug delivery.

In this work, we manufactured a polymeric device for multi-drug transscleral delivery to the posterior segment of the eye at independently controlled release rates (Fig. 1). The device comprises a microfabricated reservoir, controlled-release cover and drug formulations, which were made of photopolymeized tri(ethyleneglycol)dimethacrylate (TEGDM) and poly(ethyleneglycol)dimethacrylate (PEGDM). Here, we show that the release of multiple drugs can be tuned by changing the formulations of the drug as well as the covering, and demonstrate the transport of drugs into the ocular tissue in rats using fluorescents.

2. Materials and methods

2.1. Materials

PEGDM (*Mn* 750), TEGDM (*Mw* 286.3) and 2-hydroxy-2-methylpropiophenone were purchased from Aldrich (USA). Polydimethylsiloxane (PDMS), fluorescein (FL, *Mw* 332.31), rhodamine-B (Rho, *Mw* 479.02) and 4,6-diamidino-2-phenylindole dihydrochloride (DAPI, *Mw* 350.25) were purchased from Wako (Japan).

2.2. Device fabrication

The device consists of a reservoir that can contain different types of sustained release formulations and is sealed with a controlled release cover (Fig. 1c). PEGDM and TEGDM including 1% 2-hydroxy-2-methylpropiophenone as a photoinitiator were used for device materials. For the preparation of the reservoir, TEGDM prepolymer was poured into the PDMS mold fabricated via a microfabrication technique using a microprocessing machine (MicroMC-2, PMT Co.) (Supplementary Fig. S.1), and photopolymerized for 3 min with UV light (HLR400F-22, Sen Lights) at an intensity of 7.4 mW cm^{-2}. After loading the drugs, a reservoir cover was prepared by applying a prepolymer mixture of the required concentrations of PEGDM and TEGDM to the reservoir, followed by UV curing for 3 min. For the preparation of the fluorescent formulations, the fluorescents were combined with a mixture of a predetermined ratio of PEGDM and TEGDM and poured into PDMS molds and photopolymerized for 3 min. All fluorescent formulations had a fluorescent concentration of 50 mg ml^{-1} and the volume was 1.2 μl (60 μg) or 0.4 μl (20 μg) for single-fluorescent delivery or multi-fluorescent delivery devices, respectively. The dimensions of the device were 2 mm × 2 mm × 1 mm (external) and 1.55 mm × 1.55 mm × 0.5 mm (internal; maximum loading volume, 1.2 μl). PEGDM/TEGDM prepolymer mixture ratios of 100%/0%, 80%/20%, 60%/40%, 40%/60%, 20%/80% and 0%/100% were designated as P100, P80, P60, P40, P20 and P0, respectively.

2.3. Characterization of diffusion mechanism through the PEGDM/TEGDM system

The permeability of FL in phosphate-buffered saline (PBS) (0.5 mg ml^{-1}, 20 μl) through the PEGDM/TEGDM reservoir (4 mm × 4 mm × 1.5 mm, internal) was assessed by monitoring the increase in fluorescence in the external PBS (1 ml) solution with time ($n = 5$). To characterize the diffusion mechanism through the PEGDM/TEGDM system, we determined the swelling ability of the PEGDM/TEGDM polymers. The samples (size: 5 mm × 5 mm × 2 mm) with various PEGDM/TEGDM ratios were weighed in air before (W_b) and after (W_a) immersion for 24 h in 10 ml of PBS, and the swelling ratio ($W_a/W_b \times 100$) was calculated ($n = 5$).

2.4. In vitro release study

For the single delivery study, FL was pelletized with P60 and loaded in the device, followed by sealing with P100, P60 or P40 covers. For the multiple delivery, three types of fluorescents, FL, Rho and DAPI, were pelletized each with different ratios of PEGDM/TEGDM and loaded in the device, followed by sealing with P100 or P60 covers. The devices were each incubated in 1 ml of PBS at 37 °C. To estimate the amounts of fluorescent that had diffused out of the devices, the fluorescence intensities of the PBS solutions

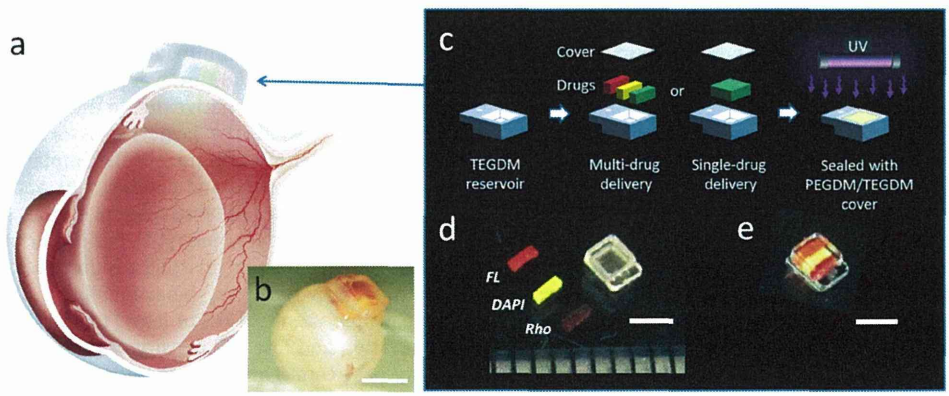

Fig. 1. (a) Schematic image of transscleral intraocular multi-drug delivery using a polymeric device placed on the sclera. (b) Photograph of the rat eye where the device was implanted on the sclera for 3 days. (c) Image shows assembling process of the device that consists of three kinds of fluorescents pelletized with PEGDM/TEGDM, a reservoir made of TEGDM and a controlled release cover made of PEGDM/TEGDM. After loading the pellets in the reservoir, the cover was sealed on the reservoir by UV curing. (d) Photographs showing three kinds of fluorescent pellets, including FL, Rho and DAPI, and a reservoir before assembling, and (e) the device after assembling. Scale bars, 2 mm.

were measured spectrofluorometrically (FluoroscanAscent; Thermo), where fluorescence excitation (ex) and emission (em) for FL, Rho and DAPI was measured at ex. 485 nm/em. 538 nm, ex. 544 nm/em. 590 nm and ex. 355 nm/em. 460 nm, respectively ($n = 6$). The PBS was replenished during the course of the release study to ensure that the concentration of fluorescent molecules was below 20% of its saturation value at all times. The results were expressed as amount determined using a standard curve.

2.5. Animal experiments

Male Sprague–Dawley rats (SLC) weighing 250–300 g were used in this study. All animals were handled in accordance with the Association for Research in Vision and Ophthalmology Statement for the Use of Animals in Ophthalmic and Vision Research after receiving approval from the Institutional Animal Care and Use Committee of the Tohoku University Environmental & Safety Committee (No. 2013MdA-218).

2.6. Implantation

The rats were anesthetized with ketamine hydrochloride (90 mg kg^{-1}) and xylazine hydrochloride (10 mg kg^{-1}). Their ocular surfaces were anesthetized with a topical instillation of 0.4% oxybuprocaine hydrochloride. A paralimbal conjunctival incision was made 1 mm from the temporal limbus. The devices were placed onto the left eyes at the sclerae. The right eyes served as controls.

2.7. In vivo release study

After implantation, the eyes were enucleated and the conjunctiva, muscle, optic nerve and the device were carefully removed. Fluorescent images were captured using a hand-held retinal camera for fluorescein angiography (Genesis-D, Kowa) to document the fluorescence distributions around the implantation site. After taking the image, the eyes were carefully separated into the retina, vitreous, lens, cornea and sclera/choroid/retinal pigment epithelium (RPE). The retina and sclera/choroid/RPE were homogenized in 100 μl of lysis buffer (1% Triton X-100 in PBS). The homogenates were centrifuged at 15,000*g* for 10 min, and the fluorescence intensity of the 80 μl of supernatant was measured spectrofluorometrically (FluoroscanAscent) ($n = 6$). For histological examination, the eyes were frozen in liquid nitrogen. A suture was placed as a landmark at the implant site of the device. After mounting the cryostat sections in a medium (Vectashield, Vector Lab), the distribution of fluorescein was observed by fluorescent microscopy (DMI6000B, Leica).

2.8. Statistical analysis

Experimental data are presented as means ± standard deviations (SD). Statistical significance was calculated with Ekuseru-Toukei 2012 (Social Survey Research Information), using the unpaired *t*-test for normally distributed isolated pairs, and the analysis of variance (ANOVA) with Tukey's test for multiple comparisons. Differences were considered significant if $p < 0.05$ (*).

3. Results

3.1. Device fabrication

The device consists of a separately fabricated TEGDM reservoir, fluorescent formulations and a PEGDM/TEGDM cover (Fig. 1c). The device was designed to deliver various formulations and dosages. In this study, sustained-release fluorescent formulations, including a single FL pellet or multiple FL/Rho/DAPI pellets (Fig. 1d), were encapsulated in the reservoir using a cover to prolong fluorescent release by limiting the rate of fluorescent dissolution within the reservoir. After loading the fluorescent pellets, the PEGDM/TEGDM prepolymer was cast over the reservoir and UV-cured to provide a seal (Fig. 1e). Because photopolymerized TEGDM is impermeable to small molecules (see below), the reservoir is a barrier that forces unidirectional fluorescent release to the sclera side.

3.2. Diffusion mechanism through the PEGDM/TEGDM system

Fig. 2a shows that the release of FL was dependent on the PEGDM/TEGDM ratio. Pure PEGDM (P100) shows the highest permeability, whereas pure TEGDM (P0) was impermeable. The release rate estimated from the slope of the curve at the initial linear state was 1296 (P100), 684 (P80), 333 (P60), 83 (P40), 35 (P20) and 0 (P0) ng day^{-1}. The release rate gradually decreased as the cumulative release approached the plateau level (10 μg ml^{-1}, maximum concentration when FL was fully released in PBS), as was seen in P100 and P80. Fig. 2b shows that the swelling ratio increased with increasing the PEGDM ratio. Fig. 2c shows the correlation of the swelling ratio, obtained from the results in Fig. 2b, with the slope obtained from the release profile results in Fig. 2a. The correlation coefficient was 0.9904, indicating almost linear correlation between the swelling ratio and release rate.

3.3. Single FL release study

Fig. 3a shows the single release profiles of FL-loaded devices that were sealed with different types of covers. Although FL-pellets without reservoir or cover showed a rapid burst-like release over 5 days, the covered devices showed a zero-order release without an initial burst. The release rate decreased with decreasing PEGDM ratio in the cover. The release rate estimated from the gradient curve for pellet, P100-, P60- and P40-covered devices were 20.7, 1.13, 0.53 and 0.10 μg day^{-1}, respectively. The results demonstrate the ability to control the release rate from a device by changing the ratio of PEGDM/TEGDM in the cover.

Devices containing FL pellet (F60) and sealed with P100, P60 and P40 covers, and pellets without reservoir or cover, were implanted onto the sclerae of rats. The devices remained at the implantation site during the experiments and were easily removed from the implantation site at the end of experiments. Routine ophthalmological examinations showed no device-related toxic effects. To demonstrate the controllability of the in vivo release of FL, images of fluorescence in the sclera after removing the device were captured by a hand-held camera (Fig. 3b). White areas corresponding to fluorescence indicate the distribution of released FL. For the pellet only, little fluorescence was observed at 1 week after implantation, probably due to the burst-like release within 5 days. For the P100-cover devices, the intensity was high at 1 week, then decreased gradually during the subsequent 3 weeks. For the P60-cover devices, the intensity was moderate for 2 weeks, then weak intensity was sustained during the remaining 2 weeks. For the P40-cover devices, weak fluorescence was sustained during 4 weeks. Trends in the fluorescence intensity were almost comparable to the in vitro release results (Fig. 3a).

Fig. 4a–d shows sectional images of an eye around the implantation site. FL (green areas) penetrated the sclera at least 1 day after implantation (Fig. 4a and c), and then reached the choroid/RPE at least 3 days after implantation (Fig. 4b and d). Intense fluorescent can be seen at the RPE, one of the blood–retinal barriers (Fig. 4d). Blurred fluorescent that passed through the RPE can be seen at the retina, indicating the passing of the molecules through the RPE into the neural retina. The amount of FL in the

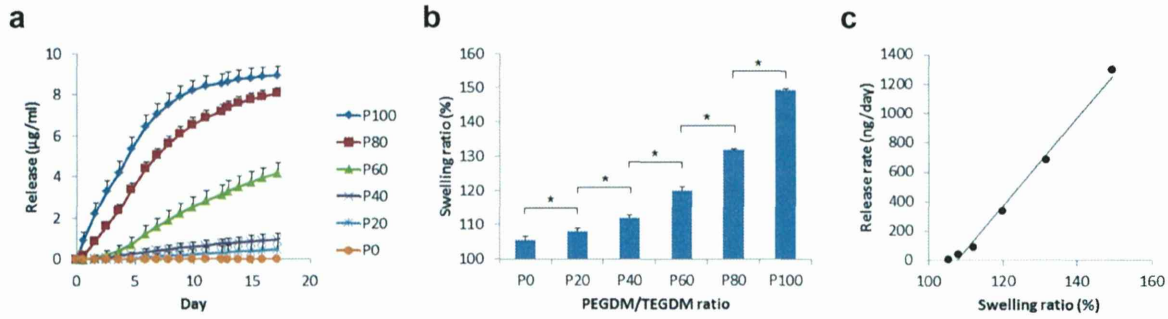

Fig. 2. (a) Permeability of FL in PBS through the PEGDM/TEGDM reservoir with various PEGDM/TEGDM ratios. The release was assessed by monitoring the increase in fluorescence in the external PBS solution with time. (b) Swelling ability in PBS of PEGDM/TEGDM polymers (size: 5 mm × 5 mm × 2 mm) with various PEGDM/TEGDM ratios. (c) Correlation between swelling ratio in (b) and release rate. Release rate was estimated from the slope of the curve of the line at the initial stable release period in (a). Values are mean ± SD. $^*p < 0.05$ (one-way analysis of variance (ANOVA) with Tukey's test).

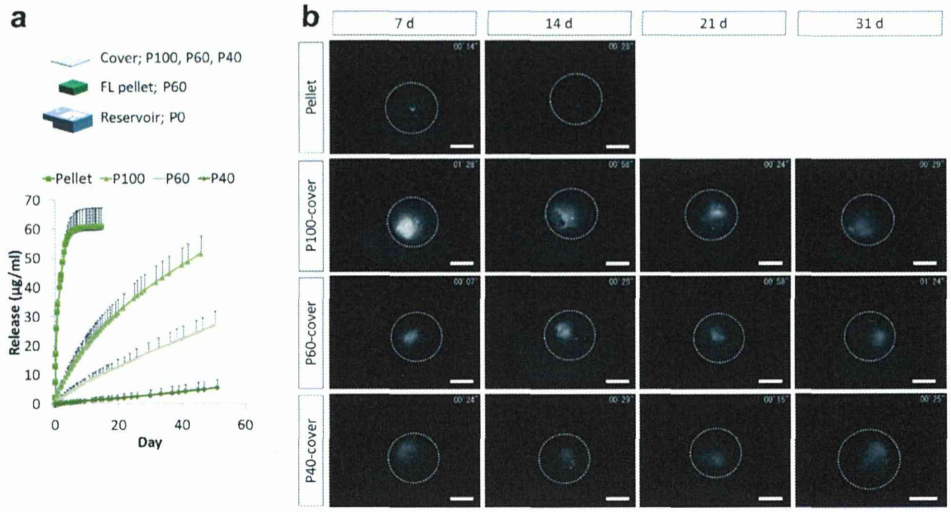

Fig. 3. (a) Release profiles of a single-drug delivery device that consists of a FL formulation pelletized with P60 and various types of cover (P100, P60 and P40), and FL pellet with no reservoir or cover. FL release was monitored spectrofluorometrically. (b) Fluorescent images of the sclera after removing the devices. Devices were implanted on the sclerae in rats for 7, 14, 21 and 31 days. White areas show released FL and circular dotted lines show the shape of the eyeball. Values are mean ± SD. Scale bars: 2 mm.

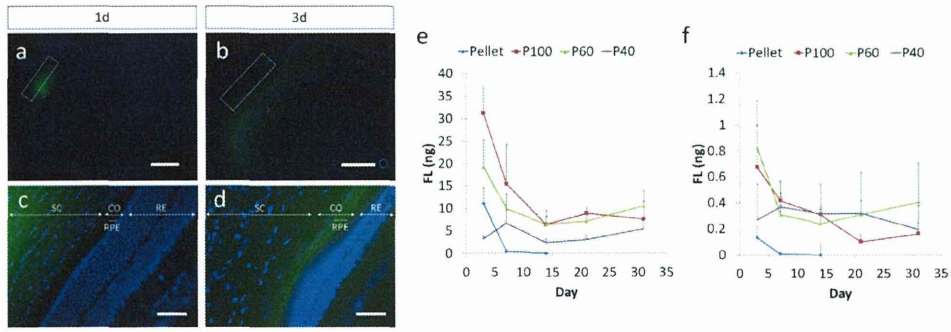

Fig. 4. The distribution of FL (green) in the retina and sclera around the implantation site (a, c) 1 day and (b, d) 3 days after implantation (square dots: device implantation site). Cell nuclei were stained with DAPI (blue). FL accumulated at RPE by day 3 after implantation and a portion of FL penetrated through the RPE and reached the retina. The amounts of FL in the sclera/choroid/RPE (e) and retinal fractions (f) during 1 month implantation. Abbreviations: sclera (SC), retinal pigment epithelium (RPE), choroid (CO) and retina (RE). Scale bars: 1 mm (a, b), 100 μm (c, d). Values are mean ± SD.

sclera/choroid/RPE, and retinal fractions during 4 weeks' implantation was measured. For the sclera/choroid/RPE fraction (Fig. 4e), the amount of FL correlated with the release profiles of the covered devices at the first week (P100 > P60 > P40). Pellet only showed almost no fluorescence after 1 week due to the burst-like release within 5 days, as is seen in Fig. 3a. From 2 weeks' implantation onwards, the amounts of FL for the P100- and P60-covered devices were at almost the same level, whereas the amount for the P40-covered device was consistently at a lower level during the successive incubation. These results are well matched with the fluorescent images on the sclera shown in Fig. 3b. For the retinal fraction (Fig. 4f), the amount of FL differed among the devices

for the first week, but was then maintained at almost the same level for each device during the following 2 weeks. Pellet only was unable to deliver FL to the retina except during the early days. After 3 weeks, the FL level for the P100-covered device was lower, while the level for the P40-covered device had decreased after 4 weeks. Although the amount of FL in the retina shows little correlation with the release profiles, the results demonstrate that fluorescent molecules released from the devices could reach the retina during the 4 weeks of implantation and the amount of FL was reduced to between 1/30 and 1/40 at the retina after passing through the sclera.

3.4. Multiple FL/Rho/DAPI release study

The simultaneous independently controlled multiple release was tested using three kinds of fluorescents, FL, Rho, and DAPI, which may mimic low-molecular-weight drugs. The device was filled with three kinds of pellets, each with different ratios of PEGDM/TEGDM. The release profiles of each pellet are shown in Supplementary Fig. S.2. DAPI pelletized with P100 (D100) was always included in the device as a constant control. FL was pelletized with P100 (F100), P70 (F70) and P60 (F60). Rho was also pelletized with P100 (R100), P70 (R70) and P60 (R60). Fig. 5a–c shows that the release rate of the molecules can be tuned by changing the composition of each pellet. For example, the release rate of FL or Rho varied as the PEGDM ratio changed (Fig. 5a vs. Fig. 5b), whereas that of DAPI was constant. When the device was sealed with a P60 cover, the absolute amount released decreased to between one-fourth and one-eighth in all of the devices compared to the P100-covered devices, but importantly, the ability to independently control the release rates of the molecules was maintained (Fig. 5d–f). If the release results were sorted for each molecule, the release kinetics of each molecule was always dependent on the PEGDM/TEGDM ratio of the pellet (Supplementary Fig. S.3). These results indicate that the release kinetics can be tuned via two independent diffusion mechanisms afforded by a sustained-release formulation and a controlled release cover.

Devices containing a combination of F60/R40/D60 pellets (device A) or F60/R60/D40 pellets (device B), sealed with a P60 cover, were implanted onto the rat sclerae. Fig. 6a–h shows the sectional images for 1 and 4 weeks after implantation. Magnified images showed fluorescence at the outer nuclear layer (ONL) in the retina and the intensity of the fluorescence correlates with device condition; device A, which releases DAPI at a faster rate than device B, shows more intense blue fluorescence in the ONL compared with device B (Fig. 6b and f). On the other hand, device B, which releases Rho at a faster rate than device A, exhibits more red fluorescence in the retina than that of device A (Fig. 6d and h). Low magnification images of the sections showed the local distribution of released fluorescents around the implantation site 1 and even 4 weeks after implantation (Fig. 6a, c, e and g). This may indicate that the released drug is specifically delivered to the retina local to the implantation site.

The amounts of fluorescence in the sclera/choroid/RPE (Fig. 7a–c) and the retina fractions (Fig. 7d–f) at 1, 2 and 4 weeks after implantation were measured. Because FL was set to release at the same rate in each device, there was no significant difference between the amount of FL detected in the fractions for device A or B (Fig. 7a and d). On the other hand, the amount of Rho in sclera/choroid/RPE and retinal fractions for device B was higher than for device A, and at 4 weeks' implantation a significant difference (p value: 0.042) can be seen in the sclera/choroid/RPE fraction (Fig. 7b). Similarly, the amount of DAPI for device A was significantly higher than for device B at 4 weeks' implantation (p value; 0.037) (Fig. 7c). There was no difference between Rho and DAPI intensities in the retina for the devices (Fig. 7e and f).

4. Discussion

We established a transscleral multi-drug delivery device with which we demonstrated the transport of low-molecular-weight compounds into the ocular tissue using fluorescents. The release of multiple drugs can be tuned by changing the formulations of the drug as well as the covering. The ability to control the release of fluorescents from the PEGDM/TEGDM system may be explained by the results of swelling tests (Fig. 2). The polymers made of short chains of TEGDM are likely to be compact, with little ability to swell, and impermeable to low-molecular-weight compounds. On the other hand, long chains of PEGDM may result in more open polymer networks, showing a greater tendency to swell, facilitating permeation of small molecules. Further, the release rate of each fluorescent differs, even when we used the same pelletized

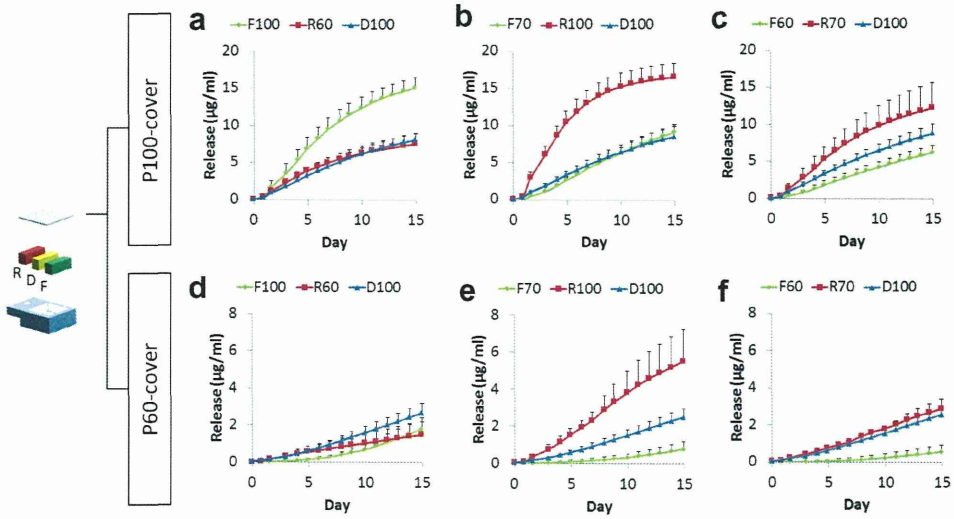

Fig. 5. (a–f) Release profiles of a multi-drug delivery device that consists of three types of fluorescent pellets (FL, Rho and DAPI, designated F, R and D, respectively, in the schematic) made of various PEGDM/TEGDM content, and two types of cover (P100 cover: (a–c), P60 cover: (d–f)). DAPI was pelletized with P100 as a constant release control. FL and Rho were pelletized with P100, P70 and P60, respectively. Values are mean ± SD.

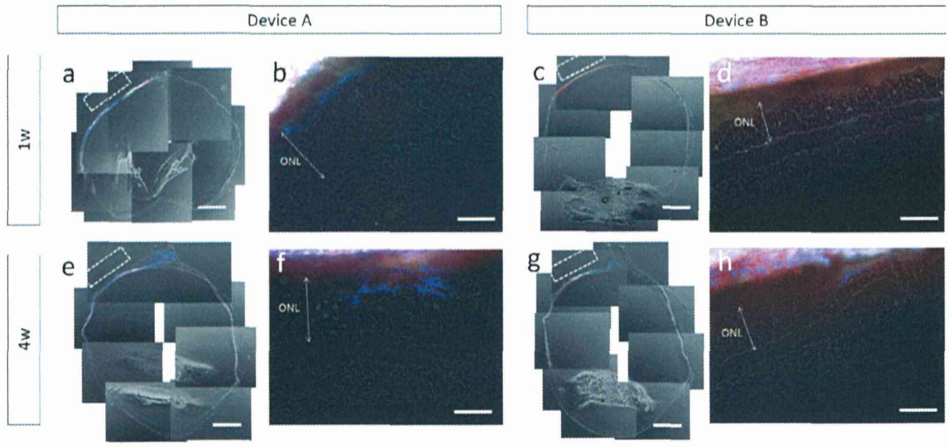

Fig. 6. (a–h) The distribution of FL (green), Rho (red) and DAPI (blue) in the retina and sclera around the implantation site 1 week (a–d) and 4 weeks (e–h) after implantation (square dots: device implantation site). Two types of devices, device A (F60/R40/D60) and B (F60/R60/D40), were used. Device A shows faster DAPI release than Rho and device B shows faster Rho release than DAPI. Magnified images (b, d, f, h) show that fluorescents reached the outer nuclear layer (ONL, double-headed allows). Scale bars, 1 mm (a, c, e, g) and 100 μm (b, d, f, h).

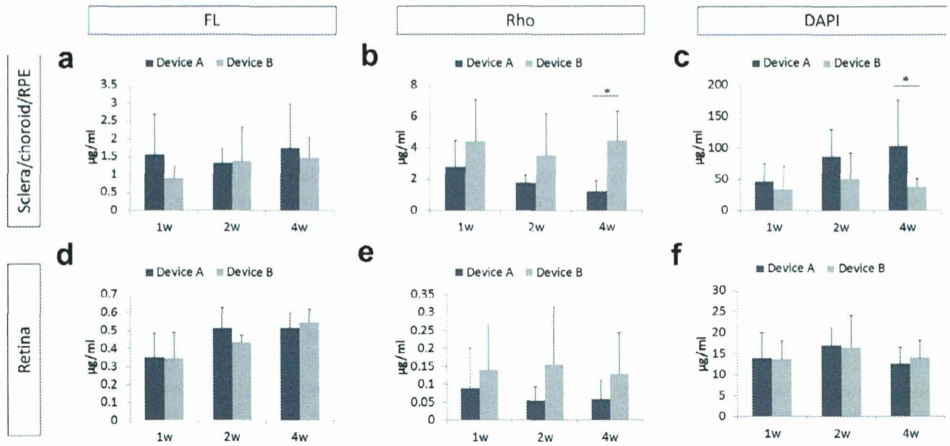

Fig. 7. The amounts of FL, Rho and DAPI in the sclera/choroid/RPE (a–c) and retinal fractions (d–f) during 4 weeks' implantation. Values are mean ± SD. $^{*}p < 0.05$ (unpaired *t*-test for normally distributed isolated pairs).

conditions (Supplementary Fig. S.2), indicating that the permeability may be influenced by the physical characteristics of the substance, such as lipophilicity, water solubility and acid–base character; FL and Rho-B are weak carboxylic acids, while DAPI is a base [33]. Therefore, we need to consider the physical characteristics of the substances and their interactions when determining the optimum PEGDM/TEGDM system for the intended drug release.

The device materials, PEGDM and TEGDM, are bio-inert and can be easily molded into different substrate shapes by UV curing [34,35]. We used a microfabrication technique because the shape and volume of the reservoir can be easily modified by an AutoCAD design. We have previously reported a reservoir-based protein-drug-release device sealed with a PEGDM cover including collagen microparticles, which served as permeation porogen for macromolecules [36]. We found that low-molecular-weight molecules can easily pass through polymerized PEGDM membrane, whereas polymerized TEGDM is impermeable to them (Fig. 2). Therefore, we newly developed a controlled release system for low-molecular-weight drugs using a PEGDM/TEGDM mixture. Some monomers of unpolymerized PEGDM and TEGDM and photoinitiator were found to elute from the device, but the amount of elution (the highest amount is 504 ng ml^{-1}) was significantly less than cytotoxically active levels (more than 391 μg ml^{-1}), and no more monomers and photoinitiator eluted after incubation in PBS for 15 days (Supplementary Fig. S.4). The PEGDM/TEGDM polymer shows almost no biodegradation 19 months after implantation on the rabbit sclera (Supplementary Fig. S.5). Additionally, the long-term implantation of the device over 4 weeks did not affect retinal function assessed by electroretinograms (Supplementary Fig. S.6). Thus, the device would appear to be stable and biocompatible for at least 1 year, and can be used to safely administer drugs by the transscleral approach without disturbing intraocular tissues.

Fluorescents were used for the analysis of drug transport into the eye from the device. Although fluorescence was observable in the ocular tissues during 4 weeks' implantation and distributed locally around the implantation site, the fluorescein concentration in the retina seemed to be almost the same in spite of the difference in the release profiles of the devices (Figs. 4f and 7e and f). This may be due to the blood–retinal barrier restricting drug transport through the RPE to the retina. Pitkanen reported that the permeability through the RPE depended on the lipophilicity and molecular weight of drugs [37]. Additionally, transporters in the RPE probably have a greater role in ocular pharmacokinetics [38]. In

fact, we observed FL accumulation around the RPE (Fig. 4d), indicating that the drug transport was restricted here. This may be one of the reasons for the constant amount of fluorescents in the retina. Additionally, this behavior might be due to the availability of fluorescents at the retina, because transport and penetration through the sclera, choroid and RPE may vary between molecules [37]. The clearance rate by blood vessels may also be different for hydrophobic and hydrophilic molecules [15]. Our device has a low-molecular-weight-impermeable reservoir that can release drugs unidirectionally to the sclera, making it less susceptible to drug elimination by conjunctival lymphatic/blood vessel clearance, so the choroid may be the primary route of clearance. Further study is needed to elucidate the factors influencing drug availability to the retina. Given that the distribution of fluorescents was concentrated at the RPE and adjacent regions, our device may be effective, especially for lesions in the vicinity of the RPE.

One of the limitations of this study is the lack of a study proving retinal neuroprotective effects of our device using clinical drugs. Previous reports show potent effective drugs, such as edaravone [39], geranylgeranylaceton [40] and unoprostone [41] against retinal degeneration in animals, whereas these drugs are administered via systemic route, topical eye drop or intravitreal injection. We are planning to perform an animal study using the clinical drugs to investigate the efficacy of our controlled transscleral multi-drug delivery system on retinal neuroprotection.

5. Conclusion

A polymeric system which can administer multiple compounds with distinct kinetics to the posterior segment of the eye was manufactured. The release of multiple compounds can be tuned by changing their formulations as well as the device covering. Furthermore, our system can be used to safely administer drugs by the transscleral approach without disturbing intraocular tissues. Strict local delivery of the drugs through our device may facilitate the administration of the drugs that would not be suitable for systemic use due to side-effects. Additionally, prolonged sustained drug release using our device would be suitable for the treatment of chronic retinal diseases. Thus, our polymeric system provides prolonged action and less invasive intraocular administration, and is expected to provide new tools for the treatment of posterior eye diseases with new therapeutic modalities.

Competing financial interests

The authors declare no conflict of interest.

Acknowledgements

This study was supported by Grant-in-Aid for Young Scientists (A) from the Ministry of Education, Culture, Sports, Science, and Technology 23680054 (N.N.), Health Labour Sciences Research Grant from the Ministry of Health Labour and Welfare H23-iryokiki-wakate-003 (N.N.), H23-kankaku-ippan-004 (T.A. and N.N.), H24-nanchitoh-ippan-067 (T.A. and N.N.), the Takeda Science Foundation (N.N.), the Tohoku University Exploratory Research Program for Young Scientists (N.N.) and Gonryo Medical Foundation (N.N.). We thank T. Kawashima, N. Kumasaka, T. Yamada and S. Ito for help with device molds preparation.

Appendix A. Supplementary data

Supplementary data associated with this article can be found, in the online version, at http://dx.doi.org/10.1016/j.actbio.2013.11.004.

References

[1] Resnikoff S, Pascolini D, Etya'ale D, Kocur I, Pararajasegaram R, Pokharel GP, et al. Global data on visual impairment in the year 2002. Bull World Health Organ 2004;82:844–51.
[2] Gragoudas ES, Adamis AP, Cunningham Jr ET, Feinsod M, Guyer DR. Pegaptanib for neovascular age-related macular degeneration. N Engl J Med 2004;351:2805–16.
[3] Kim M, Yoon BJ. Adaptive reference update (ARU) algorithm. A stochastic search algorithm for efficient optimization of multi-drug cocktails. BMC Genomics 2012;13(Suppl 6):S12.
[4] Calkins DJ. Critical pathogenic events underlying progression of neurodegeneration in glaucoma. Prog Retin Eye Res 2012;31:702–19.
[5] Fu QL, Li X, Yip HK, Shao Z, Wu W, Mi S, et al. Combined effect of brain-derived neurotrophic factor and LINGO-1 fusion protein on long-term survival of retinal ganglion cells in chronic glaucoma. Neuroscience 2009;162:375–82.
[6] Shin DH, Feldman RM, Sheu WP. Efficacy and safety of the fixed combinations latanoprost/timolol versus dorzolamide/timolol in patients with elevated intraocular pressure. Ophthalmology 2004;111:276–82.
[7] Spaide RF. Rationale for combination therapy in age-related macular degeneration. Retina 2009;29:S5–7.
[8] He S, Xia T, Wang H, Wei L, Luo X, Li X. Multiple release of polyplexes of plasmids VEGF and bFGF from electrospun fibrous scaffolds towards regeneration of mature blood vessels. Acta Biomater 2012;8:2659–69.
[9] Campochiaro PA. Potential applications for RNAi to probe pathogenesis and develop new treatments for ocular disorders. Gene Ther 2006;13:559–62.
[10] Frasson M, Picaud S, Leveillard T, Simonutti M, Mohand-Said S, Dreyfus H, et al. Glial cell line-derived neurotrophic factor induces histologic and functional protection of rod photoreceptors in the rd/rd mouse. Invest Ophthalmol Vis Sci 1999;40:2724–34.
[11] Rosenfeld PJ, Brown DM, Heier JS, Boyer DS, Kaiser PK, Chung CY, et al. Ranibizumab for neovascular age-related macular degeneration. N Engl J Med 2006;355:1419–31.
[12] Hughes PM, Olejnik O, Chang-Lin JE, Wilson CG. Topical and systemic drug delivery to the posterior segments. Adv Drug Deliv Rev 2005;57:2010–32.
[13] Del Amo EM, Urtti A. Current and future ophthalmic drug delivery systems. A shift to the posterior segment. Drug Discov Today 2008;13:135–43.
[14] Geroski DH, Edelhauser HF. Transscleral drug delivery for posterior segment disease. Adv Drug Deliv Rev 2001;52:37–48.
[15] Ranta VP, Urtti A. Transscleral drug delivery to the posterior eye: prospects of pharmacokinetic modeling. Adv Drug Deliv Rev 2006;58:1164–81.
[16] Ambati J, Adamis AP. Transscleral drug delivery to the retina and choroid. Prog Retin Eye Res 2002;21:145–51.
[17] Olsen TW, Edelhauser HF, Lim JI, Geroski DH. Human scleral permeability. Effects of age, cryotherapy, transscleral diode laser, and surgical thinning. Invest Ophthalmol Vis Sci 1995;36:1893–903.
[18] Li X, Zhang Z, Li J, Sun S, Weng Y, Chen H. Diclofenac/biodegradable polymer micelles for ocular applications. Nanoscale 2012;4:4667–73.
[19] Patel SR, Berezovsky DE, McCarey BE, Zarnitsyn V, Edelhauser HF, Prausnitz MR. Targeted administration into the suprachoroidal space using a microneedle for drug delivery to the posterior segment of the eye. Invest Ophthalmol Vis Sci 2012;53:4433–41.
[20] Aksungur P, Demirbilek M, Denkbas EB, Vandervoort J, Ludwig A, Unlu N. Development and characterization of Cyclosporine A loaded nanoparticles for ocular drug delivery: cellular toxicity, uptake, and kinetic studies. J Control Release 2011;151:286–94.
[21] Chhablani J, Nieto A, Hou H, Wu EC, Freeman WR, Sailor MJ, et al. Oxidized porous silicon particles covalently grafted with daunorubicin as a sustained intraocular drug delivery system. Invest Ophthalmol Vis Sci 2013;54:1268–79.
[22] Chen CW, Lu DW, Yeh MK, Shiau CY, Chiang CH. Novel RGD-lipid conjugate-modified liposomes for enhancing siRNA delivery in human retinal pigment epithelial cells. Int J Nanomedicine 2011;6:2567–80.
[23] Kaiser JM, Imai H, Haakenson JK, Brucklacher RM, Fox TE, Shanmugavelandy SS, et al. Nanoliposomal minocycline for ocular drug delivery. Nanomedicine 2013;9:130–40.
[24] Li X, Zhang Z, Chen H. Development and evaluation of fast forming nano-composite hydrogel for ocular delivery of diclofenac. Int J Pharm 2013;448:96–100.
[25] Wang CH, Hwang YS, Chiang PR, Shen CR, Hong WH, Hsiue GH. Extended release of bevacizumab by thermosensitive biodegradable and biocompatible hydrogel. Biomacromolecules 2012;13:40–8.
[26] Kunou N, Ogura Y, Yasukawa T, Kimura H, Miyamoto H, Honda Y, et al. Long-term sustained release of ganciclovir from biodegradable scleral implant for the treatment of cytomegalovirus retinitis. J Control Release 2000;68:263–71.
[27] Zhang H, Zhao C, Cao H, Wang G, Song L, Niu G, et al. Hyperbranched poly(amine-ester) based hydrogels for controlled multi-drug release in combination chemotherapy. Biomaterials 2010;31:5445–54.
[28] Shin HC, Alani AW, Rao DA, Rockich NC, Kwon GS. Multi-drug loaded polymeric micelles for simultaneous delivery of poorly soluble anticancer drugs. J Control Release 2009;140:294–300.
[29] Richardson TP, Peters MC, Ennett AB, Mooney DJ. Polymeric system for dual growth factor delivery. Nat Biotechnol 2001;19:1029–34.
[30] Lammers T, Subr V, Ulbrich K, Peschke P, Huber PE, Hennink WE, et al. Simultaneous delivery of doxorubicin and gemcitabine to tumors in vivo using prototypic polymeric drug carriers. Biomaterials 2009;30:3466–75.

[31] Elia R, Fuegy PW, VanDelden A, Firpo MA, Prestwich GD, Peattie RA. Stimulation of in vivo angiogenesis by in situ crosslinked, dual growth factor-loaded, glycosaminoglycan hydrogels. Biomaterials 2010;31:4630–8.
[32] Wang Y, Wang B, Qiao W, Yin T. A novel controlled release drug delivery system for multiple drugs based on electrospun nanofibers containing nanoparticles. J Pharm Sci 2010;99:4805–11.
[33] Dickens SH, Flaim GM, Floyd CJ. Effects of adhesive, base and diluent monomers on water sorption and conversion of experimental resins. Dent Mater 2010;26:675–81.
[34] Benoit DS, Durney AR, Anseth KS. Manipulations in hydrogel degradation behavior enhance osteoblast function and mineralized tissue formation. Tissue Eng 2006;12:1663–73.
[35] Kalachandra S. Influence of fillers on the water sorption of composites. Dent Mater 1989;5:283–8.
[36] Kawashima T, Nagai N, Kaji H, Kumasaka N, Onami H, Ishikawa Y, et al. A scalable controlled-release device for transscleral drug delivery to the retina. Biomaterials 2011;32:1950–6.
[37] Pitkanen L, Ranta VP, Moilanen H, Urtti A. Permeability of retinal pigment epithelium: effects of permeant molecular weight and lipophilicity. Invest Ophthalmol Vis Sci 2005;46:641–6.
[38] Mannermaa E, Vellonen KS, Urtti A. Drug transport in corneal epithelium and blood-retina barrier: emerging role of transporters in ocular pharmacokinetics. Adv Drug Deliv Rev 2006;58:1136–63.
[39] Imai S, Inokuchi Y, Nakamura S, Tsuruma K, Shimazawa M, Hara H. Systemic administration of a free radical scavenger, edaravone, protects against light-induced photoreceptor degeneration in the mouse retina. Eur J Pharmacol 2010;642:77–85.
[40] Tanito M, Kwon YW, Kondo N, Bai J, Masutani H, Nakamura H, et al. Cytoprotective effects of geranylgeranylacetone against retinal photooxidative damage. J Neurosci 2005;25:2396–404.
[41] Tsuruma K, Tanaka Y, Shimazawa M, Mashima Y, Hara H. Unoprostone reduces oxidative stress- and light-induced retinal cell death, and phagocytotic dysfunction, by activating BK channels. Mol Vis 2011;17:3556–65.

ADVANCED MATERIALS
www.advmat.de

Micropatterned Polymeric Nanosheets for Local Delivery of an Engineered Epithelial Monolayer

Toshinori Fujie, Yoshihiro Mori, Shuntaro Ito, Matsuhiko Nishizawa, Hojae Bae, Nobuhiro Nagai, Hideyuki Onami, Toshiaki Abe, Ali Khademhosseini, and Hirokazu Kaji**

Age-related macular degeneration (AMD) is a major ophthalmic disease that causes visual impairment and blindness, particularly in elderly people.[1] The pathogenesis of AMD is believed to result from the development of subretinal choroidal neovascularization triggered by an increment in secretion of vascular endothelial growth factor from retinal pigment epithelial (RPE) cells. The developing choroidal vessels invade Bruch's membrane and disrupt the RPE monolayer. Subsequently, degeneration of photoreceptors occurs and results in permanent visual loss. Hence, subretinal transplantation of RPE cells to the site of degeneration would offer an ideal treatment providing the transplanted cells could generate a monolayer, reconstruct the RPE–photoreceptor interface, and inhibit further development of choroidal vessels. Although transplantation of autologous peripheral RPE cells has been tested by injection of cell suspensions using a syringe, limited visual improvement result due to the low viability of the injected cells, and their restricted distribution and integration into the subretinal tissue.[2] In fact, we previously reported the transplantation of epithelial cells into animal models of AMD and found that similar problems to those described above occurred in the animals and that these difficulties held back further experimental development of potential therapeutic treatments.[3]

As a consequence of these problems, tissue engineering is expected to provide innovative therapeutics in regenerative medicine by directing cellular organization using microfabrication techniques.[4] Efforts are in progress towards an alternative approach which involves the local delivery of an engineered RPE monolayer using biocompatible devices. There have been several reports on the development of natural and synthetic substrates for cell delivery using collagen, poly(ethylene terephthalate) and poly(methyl methacrylate).[5] However, these engineered substrates are typically micrometers in thickness (6 μm at thinnest) and several millimeters in size. Therefore, they are not sufficiently flexible to be aspirated and injected through a conventional syringe needle into the narrow subretinal space. Thus, a large incision of the sclera and retinal tissue would be required for the injection of these rigid substrates, which would also require use of a custom-made metallic cannula with a millimeter-size rectangular opening.[5c] However, such an incision might result in leakage of vitreous fluid and lead to post-surgical infection. To minimize damage to host tissues and at the same time transplant an RPE monolayer that can withstand the required surgical manipulation, the substrates need to be simultaneously robust, extremely flexible and compliant in narrow spaces. Therefore, miniaturization of the substrates (for both thickness and size) is an important approach to achieve minimally invasive delivery of the engineered RPE monolayer.

Ultrathin polymeric films (nanosheets) are a relatively new class of soft nanomaterials that are under study in the polymer physics field.[6] Polymeric nanosheets range from tens to hundreds of nanometers thick with a very large aspect ratio (greater than 10^6) and, unlike bulk polymeric films, have unique physical properties. Their thermodynamic and mechanical properties vary in a thickness-dependent manner, resulting in high flexibility, non-covalent adhesiveness, and selective molecular permeability.[7] These properties are beneficial for biomedical applications, such as wound dressings and cellular scaffolds.[8] Previously, we demonstrated that the large surface area of

Y. Mori, S. Ito, Prof. M. Nishizawa, Prof. H. Kaji
Department of Bioengineering and Robotics
Graduate School of Engineering
Tohoku University
6–6–01 Aramaki, Aoba-ku, Sendai 980–8579, Japan
E-mail: kaji@biomems.mech.tohoku.ac.jp
Dr. T. Fujie, Prof. A. Khademhosseini
WPI-Advanced Institute for Materials Research (WPI-AIMR)
Tohoku University
2–1–1 Katahira, Aoba-ku, Sendai 980–8577, Japan
E-mail: alik@rics.bwh.harvard.edu
Prof. A. Khademhosseini
Center for Biomedical Engineering
Department of Medicine
Brigham and Women's Hospital
Harvard Medical School
Harvard-MIT Division of Health Sciences and Technology
Massachusetts Institute of Technology
Wyss Institute for Biologically Inspired Engineering
Harvard University
PRB-252, 65 Landsdowne Street, Cambridge, MA 02139, USA
Dr. T. Fujie
Department of Life Science and Medical Bioscience
School of Advanced Science and Engineering
Waseda University
TWIns, 2-2 Wakamatsu-cho, Shinjuku-ku Tokyo 162-8480, Japan
Prof. H. Bae
College of Animal Bioscience and Technology
Department of Bioindustrial Technologies
Konkuk University
Hwayang-dong, Kwangjin-gu, Seoul 143–701, Republic of Korea
Dr. N. Nagai, Dr. H. Onami, Prof. T. Abe
Division of Clinical Cell Therapy
United Centers for Advanced Research
and Translational Medicine (ART)
Tohoku University Graduate School of Medicine
2–1 Seiryo, Aoba-ku, Sendai 980–8575, Japan

DOI: 10.1002/adma.201304183

ADVANCED MATERIALS
www.advmat.de

Materials Views
www.MaterialsViews.com

polymeric nanosheets was of value for creating flexible substrates with thickness-dependent mechanical properties; these substrates could provide an adhesion interface for cardiomyocytes in a stiffness-dependent manner or could assist in the engineering of biomimetic structures.[9] Recently, we also showed that the surface property could be tailored by integration of nanoparticles or nanotubes,[10] which enhanced the morphological guidance of the skeletal muscle cells.[10b] Thus, we hypothesized that polymeric nanosheets would be an ideal platform to culture RPE cells, on which an engineered RPE monolayer is capable of withstanding deformation within a syringe needle, of recovering their original shape in the subretinal space, and of attaching to the lesion.

Here, we developed micropatterned nanosheets that supported the growth of an RPE cell line (RPE-J cells) and enabled the transplantation of the cells through a syringe needle without loss of cell viability. The micropatterned nanosheets consisted of biodegradable poly(lactic-*co*-glycolic acid) (PLGA), on which a monolayer of RPE-J cells formed. In addition, we embedded magnetic nanoparticles (MNPs, 10 nm ϕ) into the structure to improve optical visualization, manipulability, and cell morphogenesis. The viability of RPE-J cells on the micropatterned nanosheets was evaluated following the syringe manipulation step for transplantation of the engineered RPE monolayer. We also demonstrated the subretinal injectability of micropatterned nanosheets, their handling properties, and their physical stability using a swine eye model. To our knowledge, this is the first report of the development of an ultrathin flexible carrier that has the promise of minimally invasive delivery of a cellular organization into narrow tissue spaces.

Micropatterned nanosheets were prepared on poly(vinyl alcohol) (PVA)-coated substrates by a combination of a spincoating and microcontact printing technique using poly(dimethyl siloxane) (PDMS) molds (see Figure S1 in the Supporting Information). Circular nanosheets consisting of PLGA and MNPs were micropatterned on either glass or SiO_2 substrates (**Figure 1**a). The shape or diameter of the micropatterned nanosheets could be varied from 300 to 1000 μm by adjusting the microstructure of the PDMS mold (Figure S2, Supporting Information). Dissolution of the PVA sacrificial layer allowed the release of the brown-colored nanosheets (Figure 1b, 500 μm ϕ). Surface profilometer measurement showed that the thickness of the micropatterned nanosheets gradually increased toward the center; the mean thickness was ca. 170 nm regardless of MNP incorporation (Figure S3, Supporting Information). The micropatterned nanosheets could be aspirated and injected through a syringe needle or an intravenous catheter due to their highly flexible structure (Movie S1, Supporting Information). Despite the incorporation of MNPs, the micropatterned nanosheets (1000 μm ϕ) were capable of deforming flexibly inside a 24 G catheter needle (470 μm inner diameter) (Figure 1c), as determined by optical and fluorescent imaging (dual-colored by the MNPs and rhodamine B), and could bend along the inner wall of the needle (Figure 1d). In our previous study, we reported that the elastic modulus of polylactide-based nanosheets was less than 5 GPa, which is lower than that of bulk polylactide materials (7–10 GPa).[11] Thus, the micropatterned PLGA nanosheets showed good flexibility and were capable of bending inside a needle without distortion or crease formation. In fact, such flexible property has a significant advantage in cell delivery, since conventional substrates consisting of synthetic polymers are relatively bulk and rigid;[5] thus, a large incision to the sclera is required for the subretinal transplantation of the synthetic substrates. The injection of micropatterned nanosheets through a syringe needle could be a minimal invasive way to reduce the incision size of the sclera and subsequent inflammatory response. It is also noteworthy that we succeeded in the preparation of nanosheets with different morphologies by applying microfabrication technique such as circles, triangles and stars by arranging the design of PDMS molds (Figure S4, Supporting Information). The morphological variation of the micropatterned nanosheets would be beneficial for arrangement of the shape of the nanosheet, depending on the physical configuration of the transplantation site.

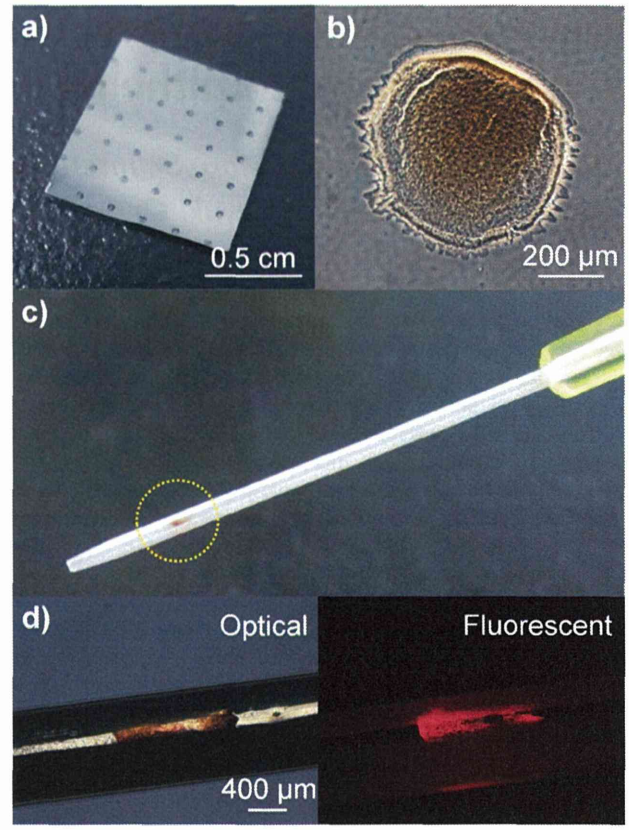

Figure 1. Typical morphology of micropatterned nanosheets. a) Macroscopic image of micropatterned nanosheets. b) Microscopic image of a single micropatterned nanosheet colored brown by the inclusion of MNPs (ϕ 500 μm). c) A micropatterned nanosheet (ϕ 1000 μm) aspirated into a 24 G intravenous catheter (470 μm inner diameter). d) Higher magnification images of the nanosheet in (c) showing that it forms a flexibly deformed structure along the inner wall of the needle.

Next, we cultured RPE-J cells on micropatterned nanosheets. We prepared the micropatterned nanosheets on PVA-coated glass substrates. Prior to seeding the cells, the surface was covered with collagen by spincoating to promote cell adhesion. Phase microscopy analysis following staining for live/dead